Everolimus Release Mechanism from Magnesium alloy Based Bioabsorbable Nanohybrid Coronary Stent

Asghar Sadeghabadi (sadeghabadi89@gmail.com)
Islamic Azad University
Seyed Khatiboleslam Sadrnezhaad
Sharif University of Technology
Azadeh Asefnejhad
Islamic Azad University
Nahid Hassanzadeh Nemati
Islamic Azad University

Research Article

Keywords: Magnesium, Nano-hybrid, Coronary stent, Degradation, Mechanism, COVID-19

Posted Date: May 11th, 2021

DOI: https://doi.org/10.21203/rs.3.rs-509597/v1

Everolimus Release Mechanism from Magnesium alloy Based Bioabsorbable Nanohybrid Coronary Stent

Asghar Sadeghabadi[1], Seyed Khatiboleslam Sadrnezhaad[2*], Azadeh Asefnejhad[1], Nahid Hassanzadeh Nemati[1]

[1]Department of Biomedical Engineering, Science and Research Branch, Islamic Azad University, Tehran, Iran

[2]Department of Materials Science and Engineering, Sharif University of Technology, Tehran, Iran

*Corresponding Author: sadrnezh@sharif.edu

ABSTRACT

The impact of magnesium degradation on Everolimus release from WE43/PLLA nano-hybrid stent was compared with cobalt-chromium L605 alloy. Effect of Mg degradation on drug release from WE43/PLLA was much higher than from L605/PLLA. SEM, UV-VIS, FTIR, pH measurement, and H_2 evolution tests determined the hybrids' property-change and drug release rate. Hydrogen evolution caused by magnesium degradation compelled Everolimus out without significant PLLA decomposition during the first 100 days, while $Mg(OH)_2$ formation caused PLLA shape change and cracking. A combined lattice/hole diffusion-dissolution mechanism governed the Everolimus release with the activation energies of 5.409 kJ/mol and 4.936 kJ/mol for the first 24 h and diffusion coefficients 6.06×10^{-10} and $3.64 \times 10^{-11} \frac{cm^2}{s}$ for the 50th to 100th days. The prolonged suppression of the hyperplasia within the smooth muscle cells by hybrid stent insertion could bring about restenosis cessation. As a result, implanting magnesium alloy stent in patients suffering from coronary artery problems and COVID19 can be more useful than current stents.

Key Words: Magnesium; Nano-hybrid; Coronary stent; Degradation; Mechanism; COVID-19

1. Introduction

One-third of all deaths in industrialized and high-stress countries are due to coronary artery atherosclerosis, and almost all older people have at least some coronary artery disease [1]. Drug eluting Stents (DES) are used in (Percutaneous Coronary Intervention) PCI for the prevention of restenosis [2]. L605 is an inactive stent alloy, resistant to corrosion with good mechanical strength. Orsiro is an L605 stent made by Biotronik Company (Germany). It has a base metal (cobalt-chromium) coated with an amorphous silicon carbide layer and then poly lactic acid (PLLA) as a carrier for Sirolimus [3]. PLLA is a semi-crystalline biodegradable polymer degraded in 3 steps and is metabolized to CO_2 and H_2O [4]. For this reason, it is widely used as a drug carrier in drug delivery and scaffolding for tissue engineering and drug-carrier and coatings for stents and other similar implants [5,6].

Corrosion-resistant DESs have, however, some problems. They limit the normal blood flow and cause an inflammatory reaction of neointima, leading to an immunological reaction, hyperplasia, and restenosis [7]. DES interfere with future surgical revascularization and their antiproliferative agent suppresses the vascular smooth muscle-cells hyperplasia and therefore results in late in-stent thrombosis [8].

Bioresorbable stents can overcome the problem by providing a temporary framework which then disappears in to the bloodstream. They eliminate the late-blockage side-effect and reduce neointimal hyperplasia, resulting in eliminating late in-stent restenosis [9,10]. The Mg stent in-vivo tests and clinical trials have proved feasibility, biocompatibility, and anti-thrombogenic property [11,12]. While maintaining the mechanical strength in the arterial vessel, Mg gradually degrades in the aqueous media and produces hydrogen and magnesium hydroxide. Magnesium hydroxide is insoluble in water, and unstable in contact with anions and acidic media. The Mg decomposition can change the Mg^{2+} concentration, pH, and H_2 partial pressure [13].

Excellent properties such as slow degradation in aqueous solution and good electrochemical properties in addition to excellent mechanical strength make the WE43 (Mg-alloy) a suitable choice for use as a cardiovascular implant [14,15]. An example is Magmaris (Biotronik Co., Germany) ballon expandable stent made of WE43 [16,17]. Its surface is completely coated with 7µm biodegradable PLLA containing Sirolimus (BIOlute) [17].

Although Magmaris clinical trials with BIOSOLVE II and BIOSOLVE III exhibited biosafety, efficacy, no death, and no apparent thrombosis [18], Mg degradation effect on drug-release remains an unknown question. More research is, hence, needed to legitimize the replacement of current stents with Sirolimus containing WE43-PLLA. The most challenging issue is high rate of degradation and local corrosion, which may lead to premature loss of strength and failure [19,20].

Sirolimus side-effect is another concern. A widely used an anti-restenosis agent, Everolimus, is pharmacokinetically better than Sirolimus, with less side-effects, good stenosis prevention, smooth muscle cell proliferation inhibition, and antiproliferative and immunosuppressive effects [21].
Everolimus was, therefore, a good choice for adding to the PLLA for coating on the WE43 substrate. This stent together with L605 alloy (control sample) was used this research. Calculation of drug release from WE43/PLLA and L605/PLLA stents revealed both the dominant mechanisms and the Mg degradation effect. All coatings had similar composition, thickness, and drug content.

2. Materials and Methods

WE43 was used as the substrate, and L605 as the control specimen. PLLA (Analytical Grade) with average weight of ~100,000 g/mol (Cas No: 33135-50-1) by Sigma-Aldrich, USA, Everolimus (Evero> 98%, CAS Registry No: 159351-69-6) of Cayman CHEMICAL (USA), Chloroform, SBF distilled water, and acetone (Iran), Ethanol and Hydrofluoric Acid, 40 wt.% (Sigma-Aldrich, USA), and NaOH, analytical grade (Merck, Germany) were used in the study. The specifications of the materials are illustrated in Table 1.

Table 1: Chemical composition of WE43, L605 (wt %), and SBF (g/L) used at pH=7.4 and T= 37 ºC.

WE43	Yttrium			Rare Earths		Zirconium		Magnesium	
	3.7-4.3			2.4-4.4		0.4 min		Balance	
L605	Cr	W	Ni	Fe	Mn	Si	C	S	P
	20	15	10	Max 3	1.5	Max 0.4	0.1	Max 0.03	Max 0.04
SBF	NaCl	KCl	$CaCl_2$	$K_2HPO_33H_2O$		Na_2CO_3	Na_2SO_4	$MgCl_26H_2O$	Tris
	8.03	0.23	0.29	0.23		0.53	0.07	0.31	6.07

A grating device by Jean Wirtz (Germany) , Digital electronic scale (AND GR-200), pH meter (DENVER INSTRUMENT (USA)), UV / VIS spectrophotometer (Germany) Analytik Jena SPECORD S600 SOFTWARE: WinASPECT®), Optical Microscope (OLYMPUS BX51 (JAPAN)), Laboratory Vacuum Hood (Laboratory Standard), SEM (LEO, Model: 1455VP, (Germany) and Agitator were used in the study.
Discs (ϕ14 × 4mm) were cut from L605 and WE43 alloys. They were polished with SiC papers in three steps and then aluminum oxide to a final level of 2000 grit, washed with distilled water, acetone, and ethanol, and then dried with hot

air. WE43 disks were treated with hydrofluoric acid for 10 h to form a protective MgF_2 layer with a thickness of approximately 1µm for slowing down the corrosion rate and better adherence of PLLA on surface. They were called F-WE43. The underside and perimeter of the specimens were carefully covered with a waterproof varnish. Their other surface was coated with PLLA (called PF-WE43) and PLLA/EVRO nanohybrid (called PEF-WE43).

PLLA/EVRO was produced by the solvent casting method which comprised of dissolving the polymer into chloroform and the drug into ethanol and then mixing the two thoroughly by a stirrer. To coat the discs, we took 0.3 ml of the homogenized solution and applied to surfaces of the F-WE43 and L605 discs. The coated area was 154 mm² and the drug dose was 1.46µg/mm² (equivalent to standard stent), and the amount of drug in each specimen was 225µg. The samples were dried in a chemical hood for 36 h to achieve a similar coating thickness. All coated discs were then transferred to a vacuum chamber for further drying for 50 h. Figure 1 illustrates the PLLA layer, the F-WE43 and L605 specimens called PE-L605 and PEF-WE43 after coating with PLLA-EVRO nanohybrid layer, and the schematic condition of the layer during degradation.

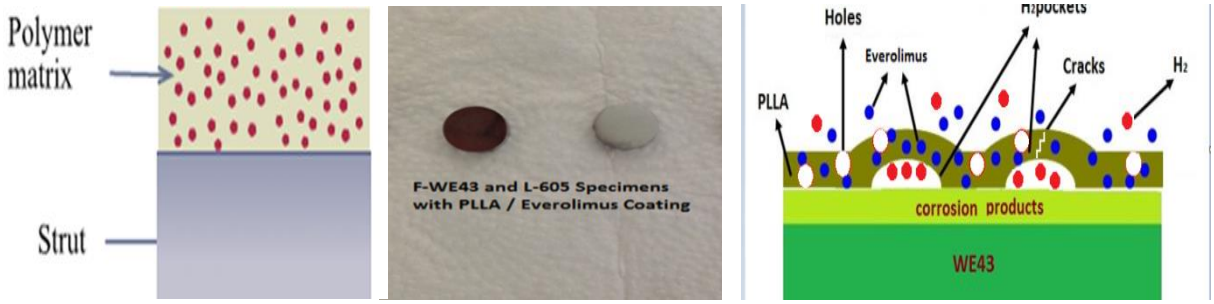

(A) (B) (C)

Figure 1: (A) Polymer-drug on a substrate, (B) PEF-WE43 and PE-L605 samples, and (C) the Mg degradation effect on the PLLA/EVRO layer.

For in-vitro release experiment, the specimens immersed in two separate containers having 10 ml of the simulated body fluid (SBF) for (a) 24 h at 1, 28, and 65°C, and (b) 100 days at the room temperature. UV-Vis spectrometer measured the Everolimus released content. The volume of the solution was kept constant by adding the same amount every time taken.

During the100-days release-tests, at each sampling stage, the solution pH was measured and recorded. A specimen of Mg alloy without polymer coating (F-WE43) was used separately as a control sample.

H_2 evolution and mass loss measurements (ASTM G1-90) from F-WE43, PF-WE43, and PEF-WE43 at 1, 28, 65ºC in the SBF indicated the amount of

produced hydrogen due to the Mg degradation. The discs were separately immersed into the SBF which was capped with a glass funnel to collect the gradually evolved hydrogen (Figure 2A). A scaled portion filled with the solution showed the gas volume. Figure 2B indicates the pH change due to the Mg degradation.

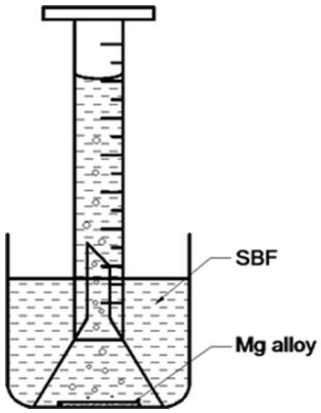

(A)

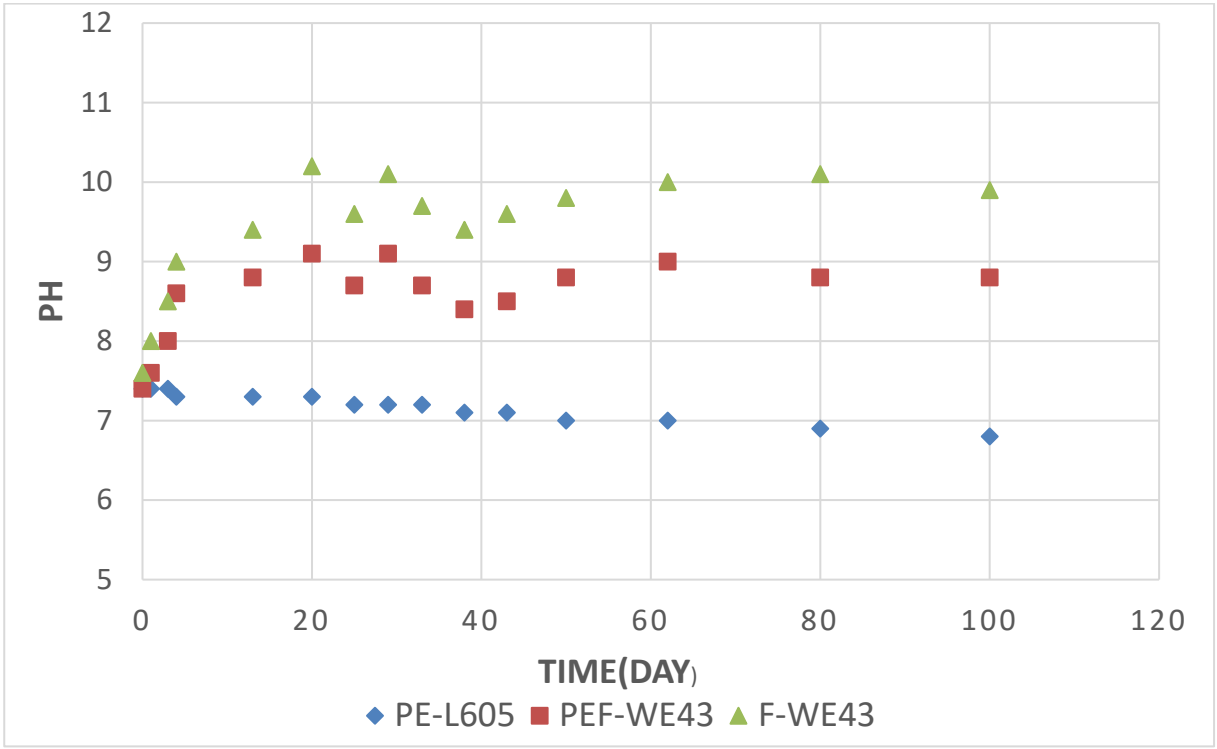

(B)

Figure 2: (A) Hydrogen evolution, and (B) pH media change of PE-L605, PEF-WE43 and F-WE43 due to the magnesium degradation during 100 days of immersion in the SBF.

The surface composition of a polished and four corroded WE43 specimens after immersion in the SBF for 2, 30, 50, and 124 h were determined by ATR-FTIR instrument. The X-ray diffraction pattern of the samples before and after 30 days of immersion was also obtained.

The effect of magnesium degradation on the metal-PLLA interface was investigated by immersing PEF-WE43 and PE-L605 specimens separately into 10 ml of SBF (pH = 7.4) for different durations. The solution was renewed regularly in each container. After immersion, the specimens were taken out, washed thoroughly with deionized water, and dried in a vacuum chamber. The PLLA surface morphology on both L605 and WE43 substrates and coatless WE43 were compared using an optical and a SEM instrument.

3. Results

Best-fit model calculations determined the release mechanism and activation energies of the involved processes below 65ºC. Because of the polymer-glass transition at 63ºC, the degradation of magnesium substrate accelerated at 65ºC and violent hydrogen evolution occurred. Above 63ºC, separation of the polymer coating from the surface of the metal substrate started.
Figure 3A shows three distinct phases in both specimens:
1. Fast release in the first 24 hours, which continued until the third day,
2. Slow release from the third day to the 43rd day, and
3. Quasi-linear release from 50th to 100th day.

The PEF-WE43 specimen showed a significantly higher release rate than the PE-L605 sample. The full PEF-WE43 release was approximately 54%, while that of PE-L605 was only 24.8%. This difference indicated the significant effect of Mg substrate degradation. The cumulative Everolimus release during the first 24 h is shown in Figure 3B.

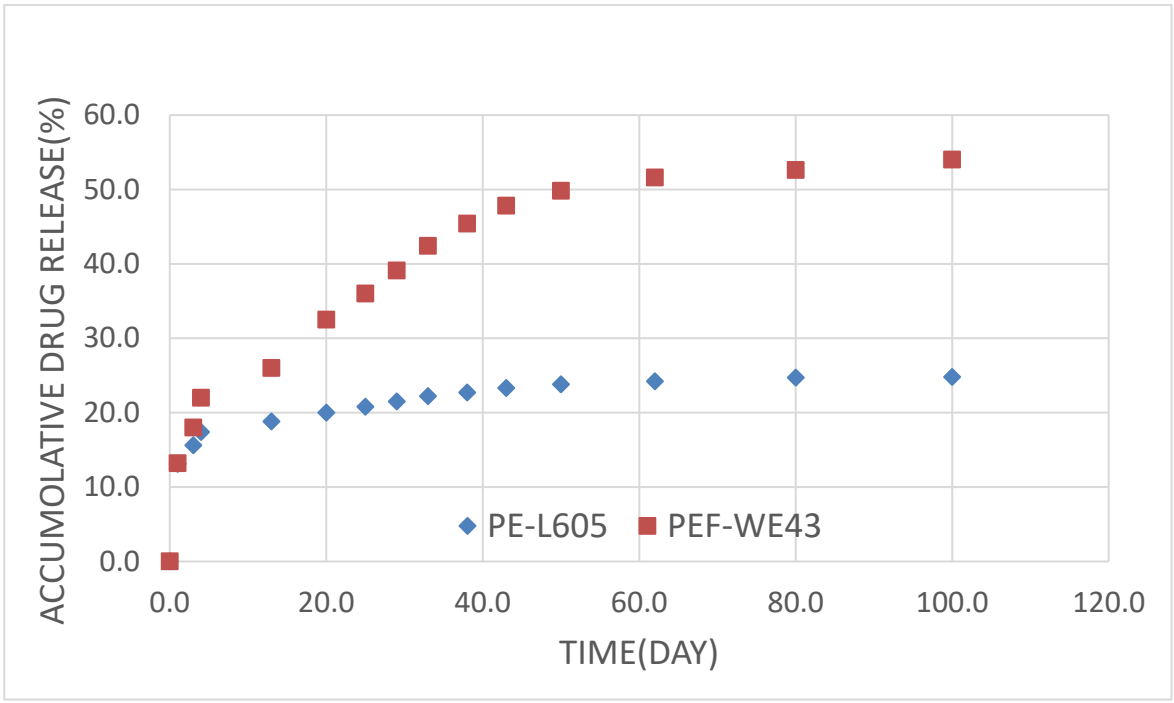

(A)

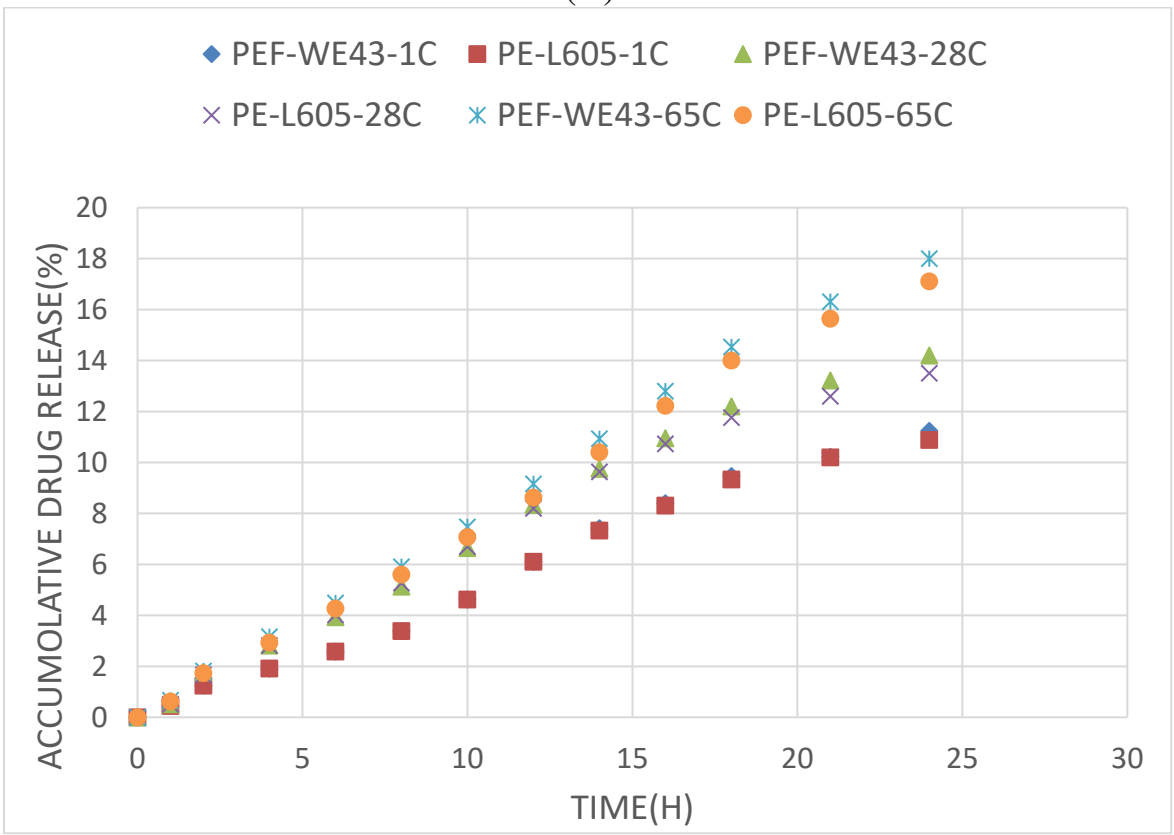

(B)

Figure 3: Cumulative Everolimus release from: (A) PE-L605 and PEF-WE43 during 100 days, and (B) PEF-WE43 and PE-L605 in the first 24 hours of immersion at 1ºC, 28ºC and 65ºC.

Changes in the media pH were monitored during the drug release process (Figure 2B). A magnesium alloy specimen without polymeric coating was used as the control specimen. For PEF-WE43, the pH had an oscillatory trend:

- rising from 7.4 to 9.1 in the first 20 days
- lowering to 8.7 on the 25th day
- reaching 9.1 on the 29th day
- decreasing to 8.8 on the 50th day
- increasing to nine on the 62nd day, and
- finally reducing to 8.8 on the 100th day.

The magnesium alloy degradation products raised the pH, and then the pH was slightly adjusted by local hydrolysis of the PLLA, which led to the release of acidic products.

In the PE-L605 stent specimen, the pH decreased slightly, with a shallow slope, and finally reached 6.8 at the end 100th day. This decreasing pH was attributed to the slow hydrolysis of PLLA, which produced intermediates resulting from decomposition with some acid-base functional groups, such as carboxylic groups, so the pH decreased slightly.

In F-WE43 (control specimen), the pH increased to 10.2 on the 20th day due to the magnesium hydroxide production. Then the downward trend took place and reached 9.4 on the 38th day. The pH increased and reached 10.1 on the 80th day. At the end of the 100th day, the pH reached 9.9. These changes were due to the magnesium's corrosive nature and the formation and dissolution of the protective coating layer. Due to the lack of PLLA coating, acidic products did not appear in this specimen, so no slight decrease in the pH was observed.

As a typical polymer coatings application for the protection of magnesium and its alloys, PLLA improves corrosion resistance and biocompatibility. However, the interaction between the polymer and the substrate magnesium alloy and the hydrogen gas produced by the degradation process often affects and weakens the protective effect of the coating. Therefore, new strategies to improve polymer coatings' performance are essential in the development and clinical application of magnesium-based implants. Relatively high corrosion rates of magnesium alloys are observed in in-vivo and SBF. This high rate of corrosion is attributed to magnesium levels' inability to passivate naturally in chloride-containing aqueous solutions at physiological pH levels and the effect of other invasive ions such as phosphates, sulfates, and carbonates. Magnesium alloys are susceptible to corrosion due to their galvanic activity among their significant constituents. These compounds include the initial phase α, the α-reactive phase, the β phase, and the alloying elements. Corrosion attacks often involve:

- galvanic coupling between the anodic and cathodic regions,

- resulting in the preferential dissolution (anodic) of the Mg matrix (phase α),
- leading to attenuation and secondary phase particles and the cathodic reaction with water.

In magnesium corrosion, small holes are formed on the surface and gradually spread throughout the surface, but due to the natural and inherent limitation of local corrosion, magnesium does not tend to form deep cavities. Mg corrosion's general formula shows that the decomposition of a magnesium atom in aqueous media produces a hydrogen molecule. Therefore, the results of the cathodic reaction mainly lead to the gradual production of hydrogen. The measured volume of hydrogen gas is equivalent to the mass loss of magnesium. The immersion test is performed according to the following equation.

$$Mg + 2H_2O \rightarrow Mg^{+2} + 2(OH)^- + H_{2(g)} \uparrow \quad (1)$$

Thus one mole of Mg consumed (24.31 g) produces the equivalent of one mole of H_2 gas (22.4L). Production rate of H_2 (V_H ml/cm²/day) is related to the rate of Mg weight loss (Δw) [22,23].

$$\Delta w = 1.085\, V_H \quad (2)$$

Therefore, from the recorded results and the above formula, the amount of mass loss in the specimens was calculated and given in Table 2. Figure 4 compares mass loss and hydrogen release from different samples at various temperatures. As can be seen, the uncoated specimen has a higher corrosion rate than the two coated specimens.

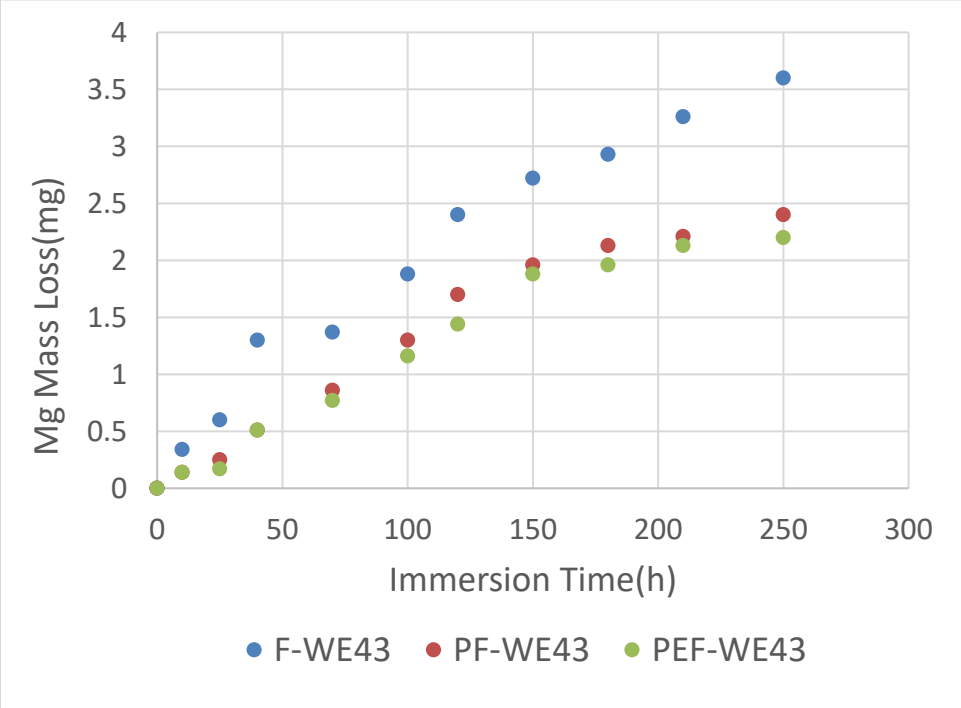

(A)

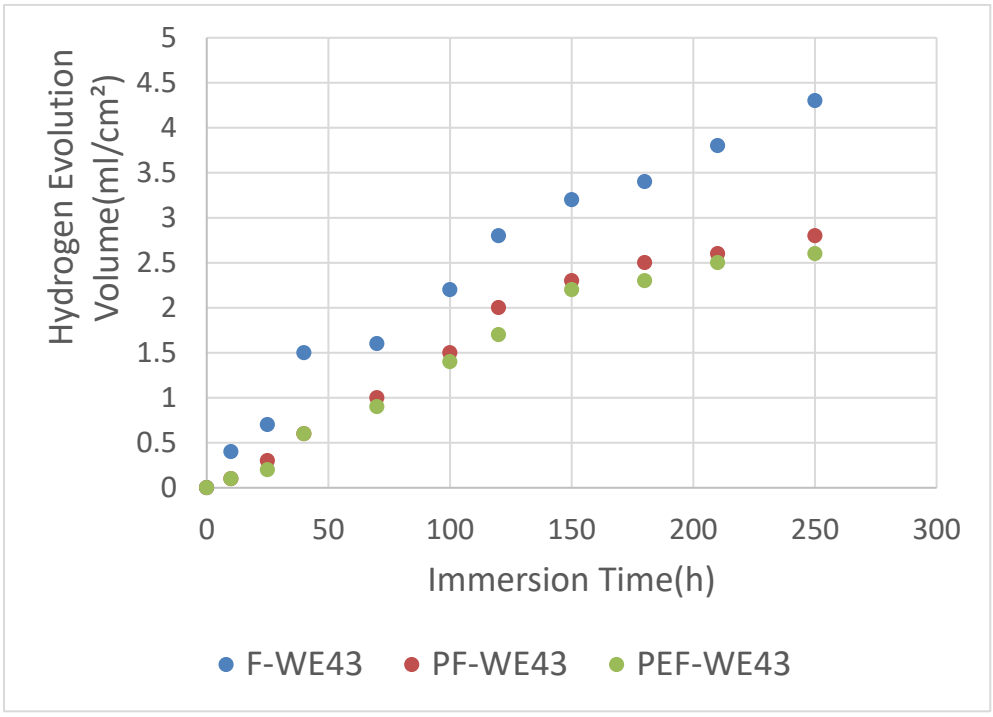
Hydrogen Evolution Volume(ml/cm²)
5
4.5
4
3.5
3
2.5
2
1.5
1
0.5
0
0
50
100
150
200
250
300
Immersion Time(h)
F-WE43
PF-WE43
PEF-WE43

(B)

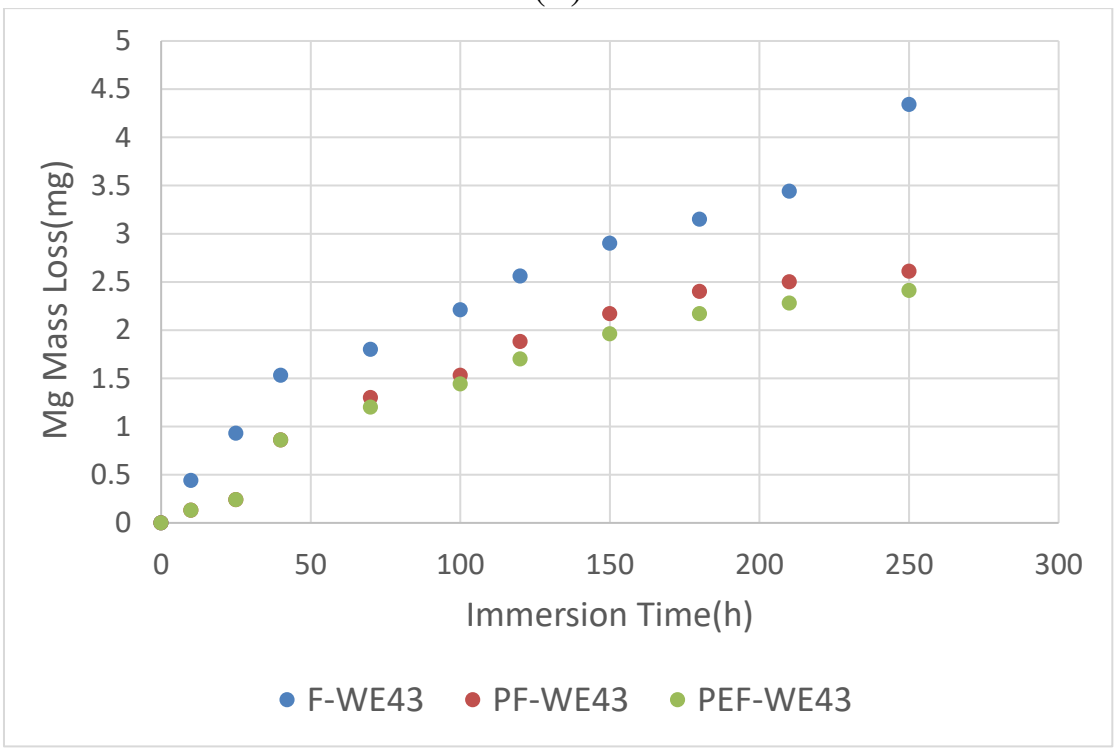
Mg Mass Loss(mg)
5
4.5
4
3.5
3
2.5
2
1.5
1
0.5
0
0
50
100
150
200
250
300
Immersion Time(h)
F-WE43
PF-WE43
PEF-WE43

(C)

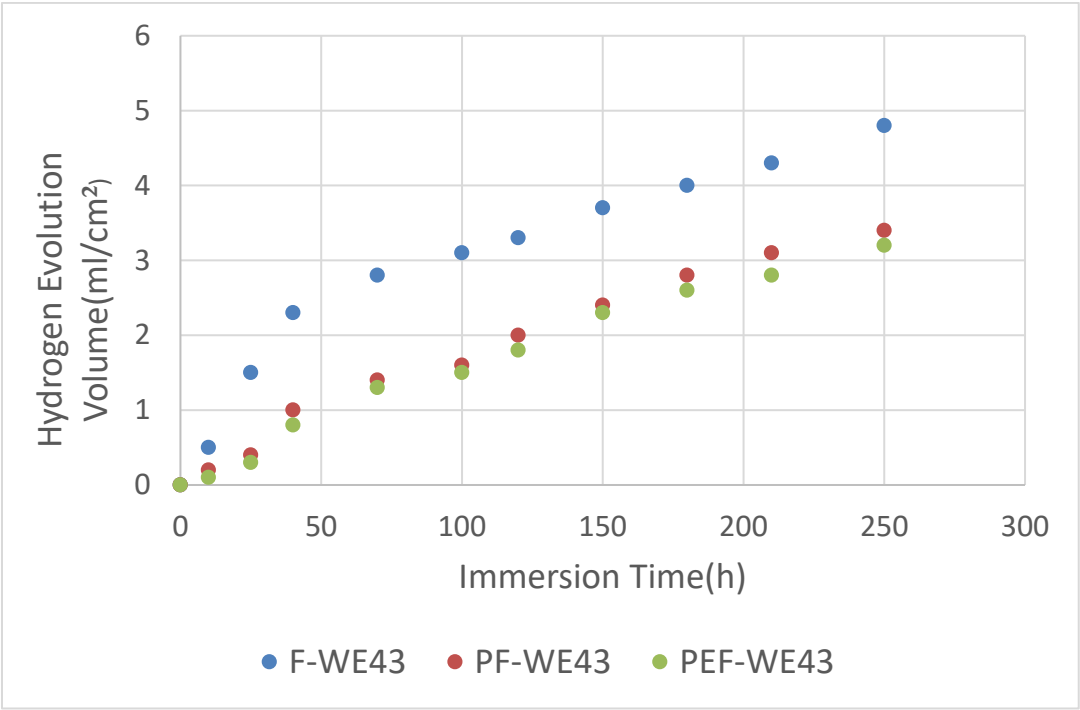
Hydrogen Evolution Volume(ml/cm²)
0
1
2
3
4
5
6
0
50
100
150
200
250
300
Immersion Time(h)
F-WE43
PF-WE43
PEF-WE43

(D)

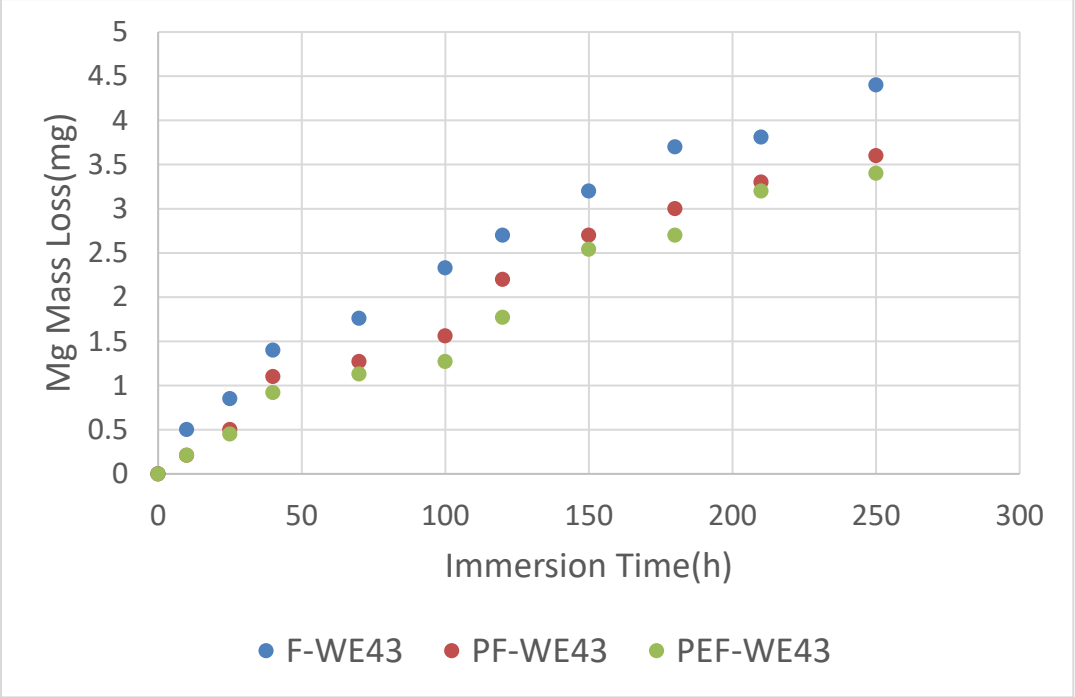
Mg Mass Loss(mg)
0
0.5
1
1.5
2
2.5
3
3.5
4
4.5
5
0
50
100
150
200
250
300
Immersion Time(h)
F-WE43
PF-WE43
PEF-WE43

(E)

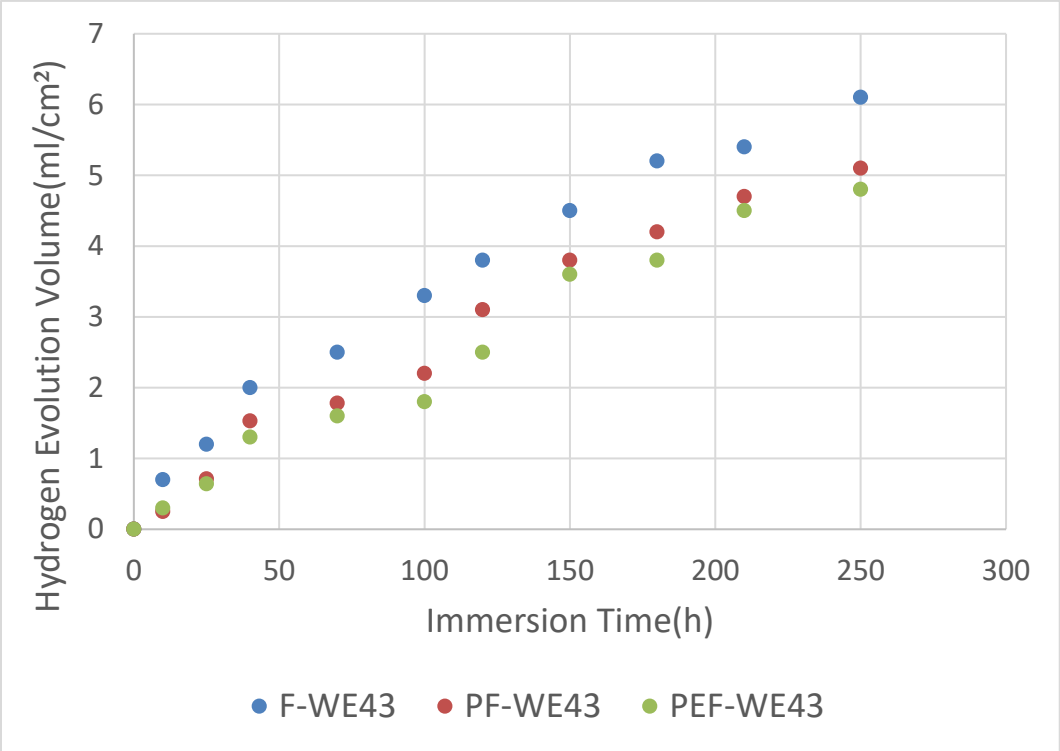

(F)

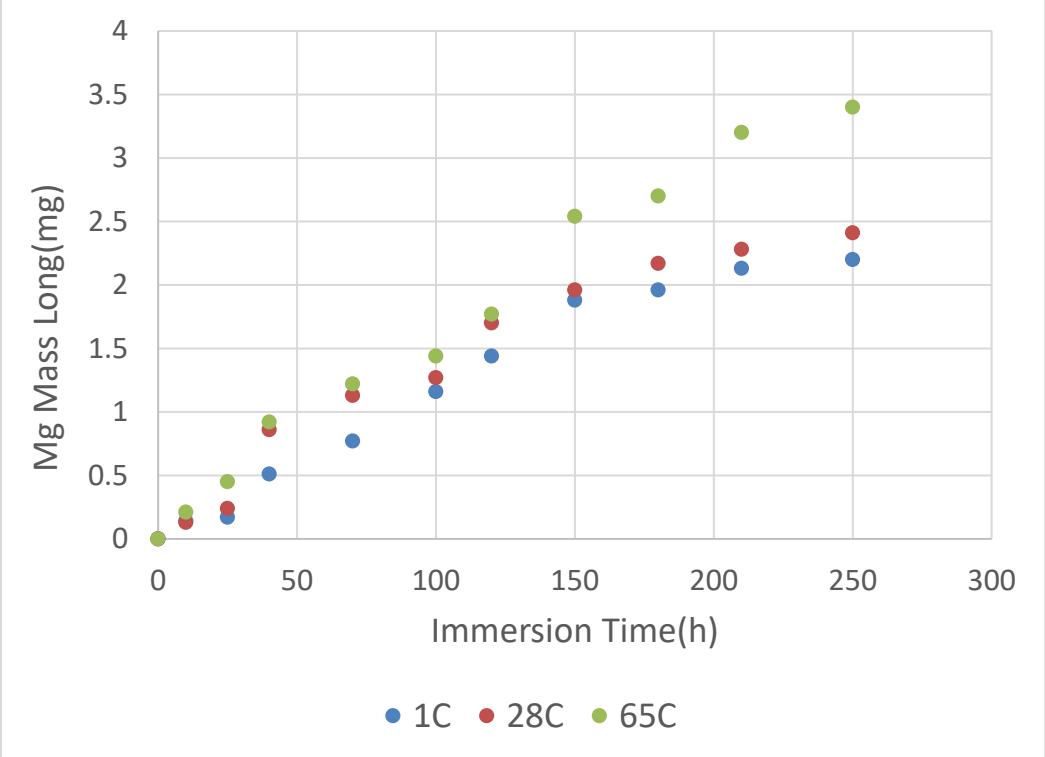

(G)

Figure 4: Mass loss (A, C, E) and hydrogen release (B, D, F) from different specimens at 1, 28, and 65℃, respectively. (G) Mass loss diagram of PEF-WE43 specimen at 1, 28, 65℃.

Table 2: Mass loss (mg) of three specimens at different temperatures in 250 h (Initial weight of each specimen averages 1.11g).

Specimen	F-WE43	PF-WE43	PEF-WE43
1 °C	3.60	2.40	2.20
28 °C	4.43	2.61	2.41
65 °C	5.30	4.30	4.00

The spectrum shown in Figure 5A indicates the presence of phosphate and carbonate anions in the corrosion layer. Phosphate adsorption bands are 1030 cm^{-1} and 580cm^{-1}. Tensile peak of 1485cm^{-1}, vibrational peak of 1430cm^{-1} and bending peak of 850cm^{-1} belonging to CO_3^{-2} ions are observable. The peak at 1600cm^{-1} shows the flexural vibrational fashion of water molecules and the hydrated layer. The peak at 710cm^{-1} corresponds to OH^-. The peak at 470cm^{-1} in the control specimen could be applied to the Mg-O tensile-vibration band. MgO has therefore formed in the sample. The presence of wide peaks of $PO_4^{-3}$and CO_3^{-2} indicates the adsorption properties of the bands, creating a weak carbonate-apatite crystal on the specimen surface. A decrease in the amount of peak size of PO_4^{-3} at 600cm^{-1} after one hour accompanied with an increase in the flexural vibration peak of water at 1600cm^{-1} shows the formation of hydrated apatite. At 124 hours, a decrease in the flexural-vibrational band of water and CO_3^{-2} is observed. This change may be due to the decrease in the concentration of CO_3^{-2} in the solution due to the release of CO_2 into the atmosphere. Therefore, the equilibrium changes towards dissolving of the carbonate layer.

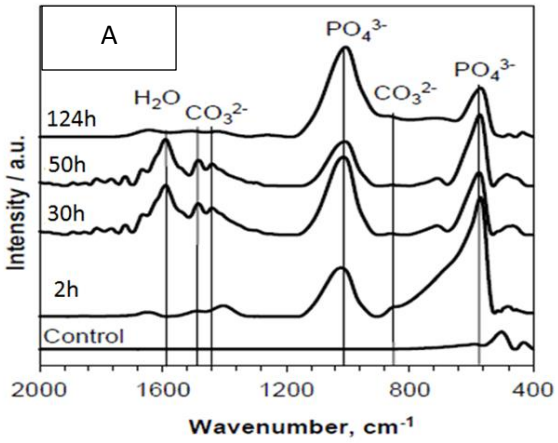

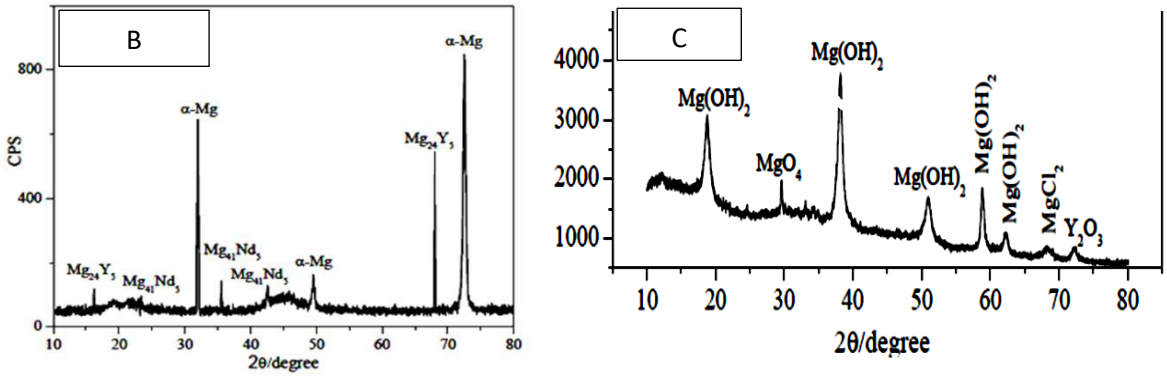

Figure 5: (A) ATR-FTIR spectrum of WE43 magnesium alloy immersed in SBF different times showing the presence of functional groups, carbonates, and phosphates. A polished WE43 specimen was used as the control specimen. (B) X-ray diffraction pattern of WE43 alloy before immersion, and (C) XRD analysis of corrosion products of WE43 alloy immersed in SBF after 30 days.

The XRD pattern for WE43 alloy shown in Figure 5B. Figure 5B shows the presence of α-Mg, $Mg_{24}Y_5$ and $Mg_{41}Nd_5$ in the produced layer. This layer also consists of Mg_{12} (RE) and Y-rich phase. These phases have positive potentials relative to the magnesium matrix, so they act as sites for production of hydrogen by the cathodic half-reaction of the corrosion. In addition, the rare earth elements in the WE43 alloy play a role in removing impurities (such as Fe, CL, S, O, H). This phenomenon can change impurities in the alloy from the state of the material in solution to intermetallic compounds. This phenomenon helps increasing the corrosion resistance.

During the WE43-SBF immersion test, severe corrosion with large cavities and cracks occurred. As the immersion time increased, all alloys were severely degraded and the surface of WE43 alloy was covered with a large amount of corrosion products. The surface was severely damaged and a large number of superficial holes were formed. When the mass loss test was completed, the corrosion products were collected from the alloy surface by a stainless steel knife. XRD analysis shown in Figure 5C indicates the corrosion products after 30 days of immersion in SBF. $Mg(OH)_2$, the main product of corrosion, was on the magnesium alloy. In WE43 alloy, MgO_4, $MgCl_2$ and Y_2O_3 can be present in the product phase, too. The oxidized Y bond at the surface of the coating film and the Y-rich region in the matrix could both effectively delay the biodegradability of the magnesium alloy [24].

Figure 6A shows a blister created by H_2 accumulation inside the PLLA coating after 6 days of immersion into the SBF. The blister grows to reach the size seen in Figure 6B and then bursts. The burst causes severe local damage to the drug-containing polymer coating, increasing EVRO expulsion. In the SEM images,

on the first day after immersion of the specimen (Figure 6C), a gradual deposition of SBF-soluble salts on the surface was observed. However, the coating was still intact. On the twentieth day of immersion (Figure 6D), large blisters of various sizes were present on the cover plus sediment. Existence of these blisters were due to penetration and passage of SBF through the polymer coating toward the substrate to cause the magnesium-water reaction for hydrogen and magnesium hydroxide production. Hydrogen has a high diffusion rate and evolves to the environment. Due to the semi-crystalline nature, the coating traps some hydrogen, which causes blistering. In other words, the formation of hydrogen bags causes microscale swelling of the coated Mg substrate. The increased surface area of the polymer coating can facilitate penetration according to the Fick's law of diffusion. The magnesium hydroxide produced causes localized scaling.

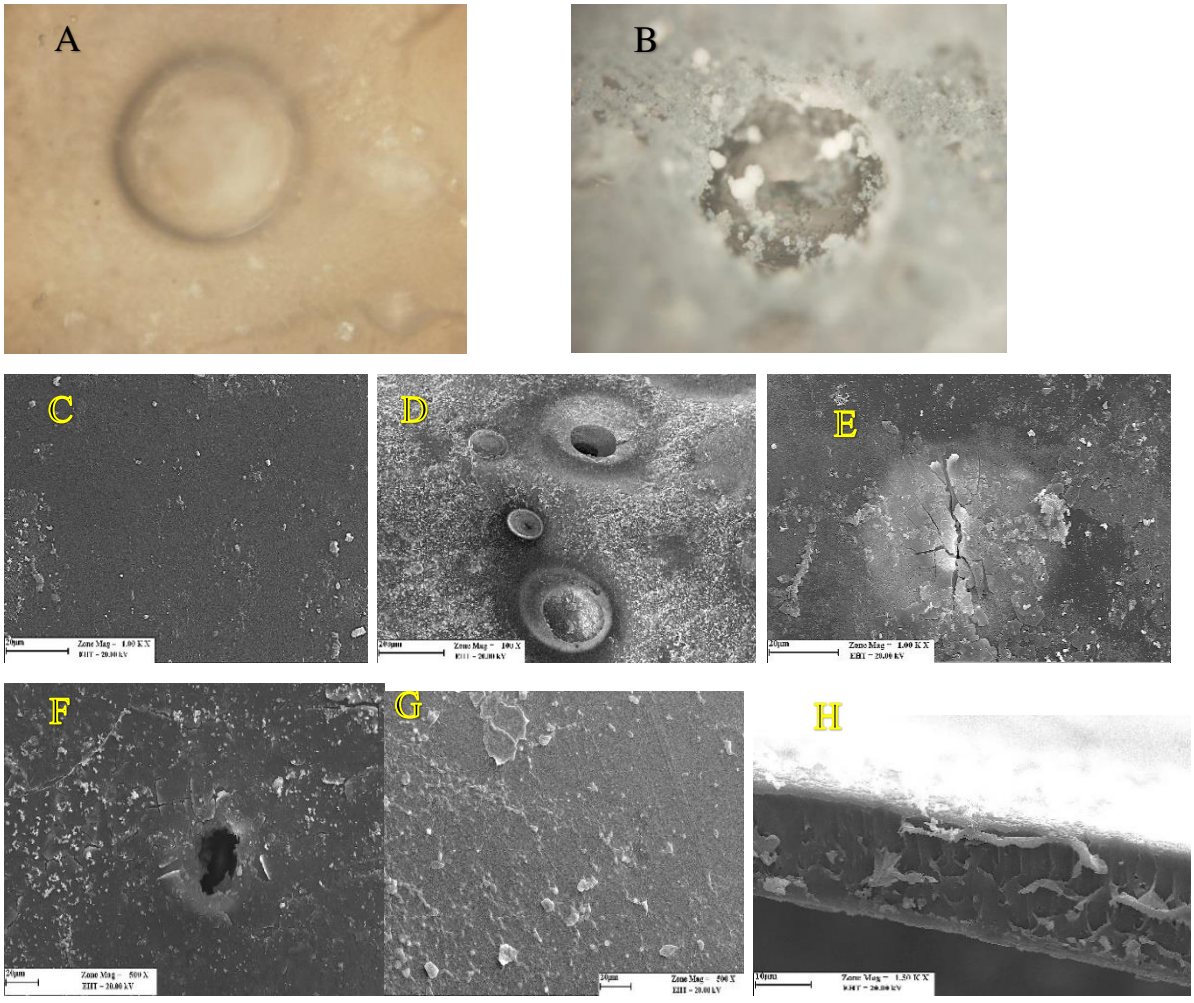

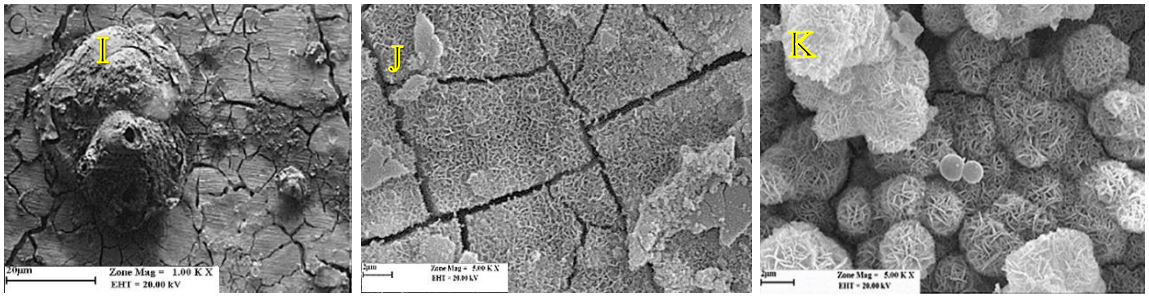

Figure 6: Blisters (A) formed by hydrogen bubbles inside the PLLA due to the magnesium-water reaction under the layer after six days (100x magnification), and (B) partial destruction of the coating after 14 days (100x magnification). And SEM micrograph of the WE43-PLLA specimen immersed in SBF for: (C) one day, (D) 20 days, (E) 30 days, and (F) 40 days. (G) L605 coating surface after 40 days immersion. (H) SEM micrograph of the cross section of the PLLA coating. (I) Corroded surface of WE43 magnesium alloy immersed in SBF for 30 h. (J and K) SEM image of the corrosion products on the PLLA coating of WE43 sample immersed for 20 days in SBF. The geometric shape and volume of the corrosion product show physical damage to the PLLA. It is, therefore, well suited to release the drug.

4. Discussion

Four stages can be considered to explain the Everolimus release mechanism:

(1) drug transfer in the PLLA solid phase,
(2) pore diffusion in the blistered PLLA layer,
(3) drug dissolution at the polymer-SBF interface, and
(4) convective Everolimus transfer into the bulk liquid away from the interface.

From the above separate steps, (1) and (2) are parallel; while (4) consecutively occurs after (3) which happens next to (2) or (1). Assuming a well-stirred solution, the forth step becomes insignificant. Step (3) is considered a first order isothermal reaction represented by a dimensionless time $\boldsymbol{g_{F_g}(X) = X}$ in which X is the fractional release defined by:

$$\boldsymbol{X = \frac{drug\ released\ mass}{overall\ loaded\ drug}} \quad (3)$$

The overall (1-2) transfer steps are considered by the quadratic term $\boldsymbol{P_{F_g}(X) = X^2}$ adopted from the well-established shrinking-core unidirectional flat system comprising a first order reaction in series with internal diffusion [25]:

$$\boldsymbol{t^* = g_{F_g}(X) + \varphi_g^2 P_{F_g}(X)} \quad (4)$$

In which $\boldsymbol{t^*}$ is the overall dimensionless time of the whole release process, $\boldsymbol{g_{F_g}}$ is the dissolution part, and the $\boldsymbol{P_{F_g}}$ is the internal diffusion share. The term $\boldsymbol{\varphi_g^2}$

called Thiele modulus is a cognation factor for the diffusion term summation with the dissolution duration [26]. Adaptation of the test data during the first 24 hours showed that drug dissolution was a controlling step at all three temperatures. Figure 7 shows the best-fit curves for both PEF-WE43 and PE-L605 samples during the first 24 hours of immersion. The activation energies for Everolimus dissolution into the SBF were determined from the Arrhenius Equation:

$$\tau = \tau_0 e^{\frac{Q}{RT}} \tag{5}$$

Where τ is the total conversion time, Q is the activation energy, R is the ideal gas constant, and T is the absolute temperature. The activation energy for the PEF-WE43 sample was 5.409 kJ/mol, while for the PE-L605 sample, it was 4.936 kJ/mol. These values are in agreement with the previously reported drug dissolution activation energies [27,28]. Calculated results for 24 hours drug release from the synthesized samples are summarized in Table 3.

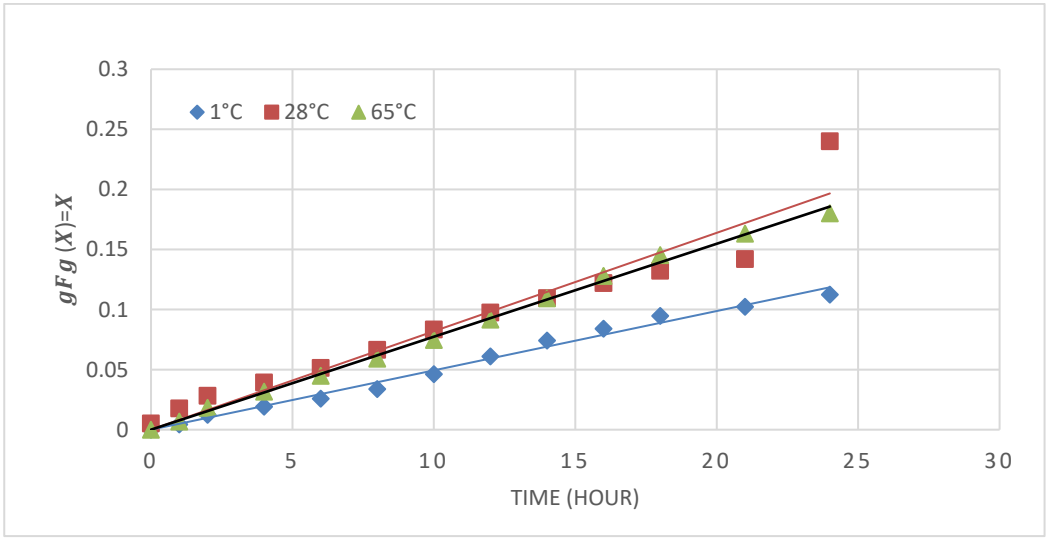

(a)

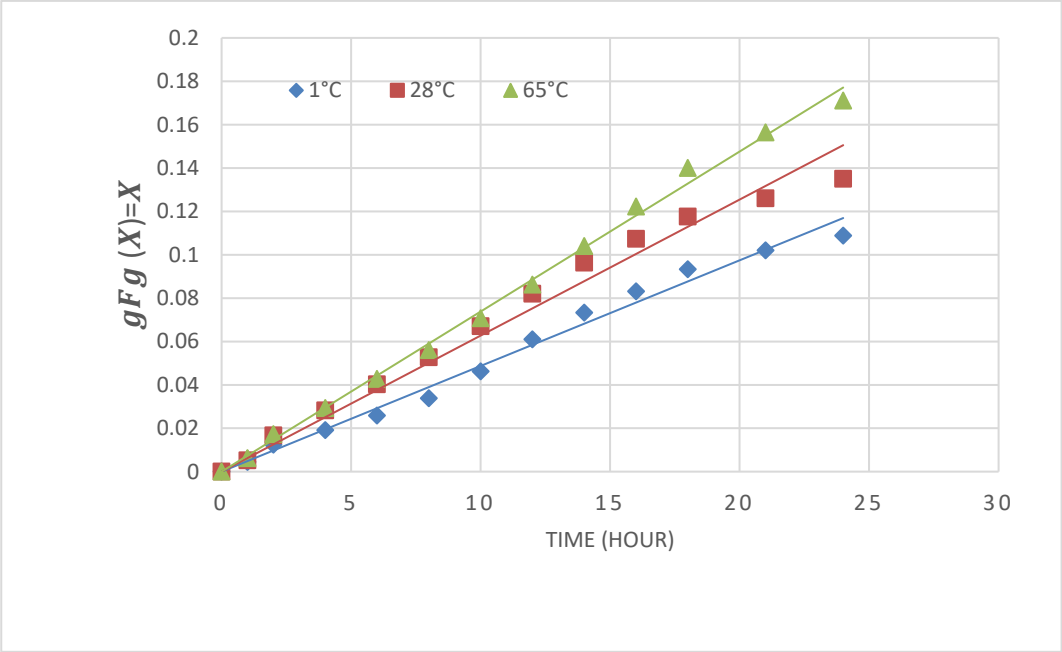

(b)

Figure 7: Comparison of the experimental release data (geometric shapes) with the model results (lines) for (a) PEF-WE43, and (b) PE-L605 samples during the first 24 hours of immersion.

Table 3: Best-fit results for 24 hours drug release from the synthesized samples.

Temperature (C°)	Dissolution Correlation		$\tau\ (h)$		Q (J/mol)	
	PEF-WE43	**PE-L605**	**PEF-WE43**	**PE-L605**	**PEF-WE43**	**PE-L605**
1	X=0.0049t R²=0.9895	X=0.0049t R²=0.9881	204.08	204.08	5409	4936
28	X=0.0063t R²=0.9804	X=0.0065t R²=0.9874	153.84	158.73		
65	X=0.0077t R²=0.9974	X=0.0074t R²=0.9965	129.87	135.14		

Matching the drug release data of PEF-WE43 for times between 4 and 43 days show a mixed control dissolution-diffusion mechanism with the equation given in the first row of Table 4. For the period between 50 and 100 days, the data indicates a mere diffusion control for PEF-WE43 sample. However, the

governing mechanism for PE-L605 after day 4 is mere diffusion with relationship constants given in Table 4.

Table 4: Best-fit kinetic data for drug release from the synthesized samples.

Sample	Time range (day)	Governing Correlation	Determination Coefficient (R^2)
PEF-WE43	$4 \leq t \leq 43$	$\frac{t}{136.99} = X + 0.1X^2$	0.9952
	$50 \leq t \leq 100$	$\frac{t}{1000} = X^2 - 0.1979$	0.9773
PE-L605	$4 \leq t \leq 43$	$\frac{t}{1666.67} = X^2 - 0.0275$	0.9971
	$50 \leq t \leq 100$	$\frac{t}{1666.67} = X^2 - 0.0542$	0.8537

From the total conversion times (τ_{dis}) inserted in the governing correlations of Table 5, one can obtain the internal diffusion coefficients from Equation (6):

$$\tau_{dis} = \frac{\rho L^2}{b k_{dis} C} \quad (6)$$

Where ρ is density, L is the layer thickness, b is the stoichiometric constant (considered one, here), k_{dis} is the dissolution rate constant, and C is the drug composition of the sample-SBF interface. The calculated values of the diffusion coefficients are given in Table 5.

Table 5: Calculated results of drug release kinetics.

Specimen	Period (days)	τ_{dis} (day)	D (cm^2/s)
PEF-WE43	50-100	1000	6.06×10^{-10}
PE-L605	50-100	16667	3.64×10^{-11}

The lower total conversion time of PEF-WE43 than PE-L605 indicates the degradation effect of Mg. The diffusion coefficient of PEF-WE43 is thus higher than PE-L605 due to faster transfer in the blistered layer. The dissolution/diffusion mechanism change from PEF-WE43 to PE-L605 indicates the latter's slower drug transfer due to the dense/non-blistered PLLA on PE-L605. The dense/non-blistered PE-L605 has a lower diffusion coefficient than PEF-WE43 at longer times. The intensification of the drug release in the PEF-

WE43 is due to three factors: alkaline environment, H_2 evolution, and corrosion products. While the evolution of H_2 has a significant consequence on increasing the drug diffusion rate, the effect of pH on drug release is small. The inactive specimen (PE-L605) has neither H_2 evolution nor alkaline medium formation.

In the coated specimens, direct contact of the PLLA with the aqueous solution causes the hydrolysis reaction catalyzed by the acidic or basic medium. The hydrolysis leads to pores and cracks in the polymer coating and more decomposition intermediates, mainly oligomers and monomers, which typically have carboxylic groups. The decomposition of the polymer is generally autocatalized by the carboxylic acid end groups collected in the cavities. It has been found that the pH inside the cavities caused by the erosion of anhydrides is between 4 and 5, while the areas far from the surface and inside the bulk are around 7.4. Even lower pH has been observed in the erosion of polymers. For example, for PLLA and similar polymers, a lower pH is observed due to higher solubility and lower PKa compared to poly (anhydride) monomers. Therefore, the higher pH of the solution accelerated the hydrolysis of PLLA in the first step. As a result, due to the production of products resulting from pH reduction, a decrease in the polymer coating was observed. In addition, a solution with a pH range of 7.4-10 could neutralize the acidic products of the decomposition in the micro medium and thus may prevent the autocatalysis of the final carboxylic acid groups on the gap (opening) of the polymer chain. A previous study showed that the biodegradation rate of PLLA was flattened in a medium alkaline medium with pH = 9.24 (zero decomposition) while the polymer was decomposed in media at pH = 5.0. Based on previous findings, it can be inferred that PLLA hydrolysis in the play environment with pH <9.7 may not progress [13].

From the amount of hydrogen produced from the three specimens, it is clear that the production of hydrogen in the uncoated specimen was significantly higher than the two coated specimens. This difference indicates that more magnesium has reacted with the SBF, indicating greater exposure to the solution. It is observed that the uncoated specimen lost a higher mass than the two coated specimens. Nevertheless, the amount of mass lost in the two specimens is close to each other. Therefore, it is clear that the use of PLLA coating can control the corrosion rate of the substrate and the production of hydrogen gas. This process will prolong the absorption of the implant in the body. Of course, this operation needs to consider many parameters such as coating thickness, type of coating technique, polymer concentration, polymer crystallinity, polymer purity, and polymer-drug homogeneity.

The experiments showed that the loaded drug had little effect on substrate corrosion. The PLLA served as a temporary absorbable protective coating and a

suitable drug carrier. In addition to slowing down the corrosion rate and controlling the drug release, the PLLA maintained the corrosion products underneath the layer. This polymer was hydrolyzed in 24 months, but the magnesium alloy decomposed in 12 months. The degradable Mg coating with the PLLA was, therefore, proposed to avoid release of the metallic debris inside the blood. This way, blood fluids could penetrate to the polymer and reach the base metal to react with the Mg. Produced hydrogen diffuses through the polymer layer and leaves the stent. By substrate decomposition, the PLLA hydrolysis will also occur and the coating begins to degrade.

5. Conclusions

The EVRO release kinetics of biodegradable WE43 alloy based specimen were studied in SBF system in comparison with the passive L605 specimen. The following conclusions were obtained from the investigation:

1. In-vitro drug release kinetics can be increased by gradual production of hydrogen and corrosion products formed during magnesium-based substrate degradation. Hydrogen gas has a high transfer rate; so it helps the drug release speed. Most magnesium corrosion products have a sharp-edge special shape that cause physical damage to the PLLA coating and furtherance of the EVRO release rate from the F-WE43 specimen. Effect of the weak alkaline pH was negligible on the EVRO release peed.

2. Due to the greater release of the drug in the magnesium alloy specimen loaded with EVRO, it is predicted that the magnesium base stent will be able to prevent smooth muscle cell proliferation (SMCs) and restenosis for a longer period of time compared to non-active substrates drug-loaded (L605).

3. The creation of an alkaline environment due to the destruction of the magnesium substrate may affect the effectiveness of the drug. This effect is, however, not severe.

4. In the first 24 h, the prevailing release mechanism is dissolution with an activation energy of 5.409 kJ/mol for the coated WE43 specimen and 4.936 kJ/mol for the coated L605 alloy. By increasing the time, the release mechanism tends gradually to convert to internal diffusion due to the difficulties arising from lowering of the drug composition in the PLLA layer. The Everolimus diffusion coefficient is $6.06 \times 10^{-10}\ \frac{\mathrm{cm}^2}{\mathrm{s}}$ for the Mg based sample and $3.64 \times 10^{-11}\ \frac{\mathrm{cm}^2}{\mathrm{s}}$ for the Co-Cr based sample during the period of 50 to 100 days from the release start.

5. In the Mg-based sample, the dominant release mechanism is dissolution until the end of the fourth day; from the fourth day to day 43 mixed (dissolution + diffusion) and then until the end of the 100-day period, it is mere diffusion. For Co-Cr based sample, the mechanism during the first day is dissolution and then until the end of 100-day, it is merely diffusion with a lower coefficient.

Many factors can affect PLLA erosion. At local pH > 10, a damage occurs by H_2 plus $Mg(OH)_2$. Both factors increase the rate of PLLA degradation and drug diffusion. Intermediate products of the substrate react with the coating and accelerates PLLA degradation. In addition, scaly corrosion products cause physical damage to the PLLA, which effects the release rate.

6. Patients suffering from COVID19 experience a drastic decrease in their blood oxygen content due respiratory damages. On the other hand, coronary arteries diverging from trailhead inside aorta pump highest oxygen content into heart muscles. As such, patients with heart coronary artery atherosclerosis are prone to higher risk in case of suffering from COVID 19. Among the other reasons contributing to this condition is the inadequate blood flow with low oxygen content Consequently, suffering from MI and mortality rate will be on higher among this group of patients.

We could demonstrate that magnesium stent has higher drug release than Co-Cr stent. Therefore, it has more capability in preventing re-stenosis. Furthermore, magnesium stent is bioabsorbable and is gradually resorbed in body and at the same time, coronary artery vessel remains opened so that blood flow is restored

As a result, implanting magnesium alloy stent patients suffering from coronary artery problems and COVID19 can be more useful than current stents.

It is noted that this study was performed mainly in SBF solution, the composition of which is very different from a real dynamic biofluid system.

Many research centers and biomedical engineering companies are currently working on the bioabsorbable stents. These activities include the development of more biocompatible materials, ultrathin stents, Nanomedicine usage, and better scaffold design to overcome existing limitations. We believe that bioabsorbable stents based on magnesium alloy are the devices most associated with innovation in coronary interventions and may ultimately lead to long-term clinical benefits and ultimate success.

6. Acknowledgements

The authors acknowledge the Iran National Science Foundation for general support of the research.

7. Data availability

The raw data required to reproduce these findings are available upon electronic/written request.

References

[1]. Dennis Kasper, Anthony Fauci, Stephen Hauser, Dan Longo, J. Larry Jameson, Joseph Loscalzo, "Harrisons' Principles of Internal Medicine", 19th.ed, McGraw-Hill Education, 2015.

[2]. Jason Foerst, Marc Vorpahl, Rainer Wessely, "Evolution of coronary stents: From bare metal stents to fully biodegradable drug eluting stents". Combination Products in Therapy, 3, Pages 9-24, 2013.

[3]. Michael J. Lipinski, Ron Waksman"A comparison of the ultrathin Orsiro Hybrid Sirolimus-eluting stent with contemporary drug-eluting stents: A meta-analysis of randomized controlled trials", Cardiovascular Revascularization Medicine, Volume 19, Issue 1, Part A, Pages 5-11, 2018.

[4]. Pegueroles Neyra, Marta, "Fabrication and surface modification of PLLA films for cardiovascular Applications", Project Pages 1-88, ETSEIB, 2014.

[5]. Ming Wu, Lothar Kleiner, Fuh-Wei Tang, Syed Hossainy, Martyn C.Davies and Clive J. Rberts, "Surface characterization of Poly(Lactic acid)/Everolimus and Poly(ethylene vinyl alcohol)/ Everolimus stent" Drug delivery,Volume 17, Issue 6, Pages 376-384, 2010.

[6]. A. Raval, Jigisha K parikh, Chhaya Enginner, "Mechanism of controlled release kinetics from medical devices" Brazilian Journal of Chemical Engineering, volume 27(2), Pages 211-225, 2010.

[7]. M Chadi Alraies, Fahed Darmoch, Ramyashree tumm ala, Ron Waksman, "Diagnosis and management challenges of in-stent restenosis in coronary arteries", World Journal of Cardiology, volume 9, issue8, Page 640, 2017.

[8]. Jian Zhao, Zhichao Mo, Fangfang Guo, Donglu Shi, Qian Qian Han, Qing Liu "Drug loaded Nano particle coating on totally bioresorbable PLLA stents to prevent in-stent restenosis", Society for Biomaterials, 106(1), Pages: 88-95 2016.

[9]. Damiano Regazzoli, Pier Pasquale, Antonio Colombo, Azeem Latib. "New generation bioresorbable scaffold technologies: an update on novel devices and clinical results", Journal of Thoracic Disease, Suppl9, Pages 979-985, 2017.

[10]. Hiroyuki Jinnouchi, Sho Torii, Aloke V. Finn “Fully bioresorbable vascular scaffolds: Lessons learned and future directions”, Nature Reviews Cardiology, Volume 16, Pages 286-304, 2018.

[11]. Enrico cerrato , Umberto Barbero, Jorge A Gil Romero, Giorgo Quadri, Hernan Mejia-Renteria, Francesco Tomassini, Fabio Ferrari, Ferdinando Varbella, Nieves Gonzalo, Javier Escaned “ Magmaris Resorbable Magnesium Scaffold: State-of-art review” Future Cardiology,15(4), Pages 267-279, 2019.

[12]. Carlos M. Campos, Takashi Muramatsu, Javaid Iqbal, “ Bioresorbable Drug-Eluting Magnesium-Alloy scaffold for treatment of coronary artery disease”, International journal of molecular science, Volume 14, Issue 12, Pages:24492-24500, 2013.

[13]. Yongjuan Shi, Jia Pei, Lei Zhang, Byung Kook Lee, Yeonhee Yun, Jian Zhang, Zhonghua Li, Song Gu, Kinam Park, Guangyin Yuan” Understanding the effect of magnesium degradation on drug release and anti-proliferation on smooth muscle cells for magnesium-based drug eluting stents” Corrosion Science,Volume 123.15, Pages 297-309, 2017.

[14]. ElenaLukyanova, Yuri Estrin “Features of *in vitro* and *in vivo* behavior of magnesium alloy WE43”, Material, Volume 215, Pages 308-311, 2018.

[15]. Mario Alberto Ascencio Pinedo, “Investigation of the corrosion behavior of bare and polypyrrole-coated WE43 magnesium alloy for the development of biodegradable implants, Department of chemical engineering, Mcgill university, Montreal Canada, 2016.

[16]. John Bennett, Quentin De Hemptinne, keir MC Cutcheon, “Magmaris resorbable magnesium scaffold for the treatment of coronary heart disease: Overview of its safety and efficacy, Expert Review of Medical Devices, Volume 16, Issue 9, Pages 757-769, 2019.

[17]. Claudio Rapetto, Massimo Leoncini, “Magmaris: a new generation metallic sirolimus-eluting fully bioresorbable scaffold: present status and future perspectives” Journal of Thoracic Disease, (Suppl 9), Pages 903-913, 2017.

[18]. Alexander Hideo-Kajita, Micheal Haude, “Comparison of clinical outcomes between Magmaris and Orsiro drug eluting stent at 12months: Pooled patient level analysis from BIOSOLVE II-III and BIOFLOW II trials” International Journal of Cardiology, Volume 300, Pages 60-65, 1, 2020.

[19]. MS Uddin, Colin Hall, Peter Murphy, “Surface treatments for controlling corrosion rate of biodegradable Mg and Mg-based alloy implants”, Science and Technology of Advanced Materials, School of engineering south Australia, Volume 16, Issue 5, 2015.

[20]. Emmet Galvin, Swarna Jaiswal, Caitriona Lally, Bryan MACdonald, Brendan Duffy “In vitro Corrosion and Biological Assessment of Bioabsorbable

WE43 Mg Alloy Specimens", Journal of Manufacturing and materials processing, Volume 1, Issue 1, 2017.
[21]. Lisette Okkels Jensen MD, Per Thayssen MD, Evald Hoj Christiansen MD, Micheal Maeng MD, "Safety and Efficacy of Everolimus Versus Sirolimus Eluting Stents: 5-Year Results From SORT OUT IV" , Journal of the American College of Cardiology, Volume 67, ISSUE 7, 23, Pages 751-762, 2016.
[22]. Jorge Gonzalez, Frank, "Magnesium degradation under physiological condition-Best practice", Bioactive material, Volume 3, Issue 2, Pages 174-185, 2018.
[23]. Yuichi Ozaki, Ron Waskman, "Second-Generation Drug-Eluting Resorbable Magnesium Scaffold: Review of the Clinical Evidence", Cardiovascular Revascularization Medicine, volume 21, Issue 1, 2020.
[24]. Li Jiang , Fang Xu, Zhen Xu, Yu Chen, Xuehua Zhou, Guoying Wei, Hongliang Ge, "Biodegradation of AZ31 and WE43 Magnesium Alloys in simulated body fluids", Int. J. Electrochem. Sci, Volume 10, Pages 10422-10432, 2015.
[25]. S.K. Sadrnezhaad, A. Gharavi, A. Namazi, "Software for kinetic process simulation", IJE Transactions A, Vol. 16, No.1, Pages 59-70. 2003.

[26]. Mazet, N., "Modeling of Gas-Solid Reactions. 1. Nonporous Solids", International Chemical Engineering, Vol. 32, No. 2, Pages 271-284, 1992.

[27]. Marjorie Caroline Liberato Cavalcanti Freire, Francisco Alexandrino, Henrique Rodrigues Marcelino, Paulo Henrique de Souza Picciani, Kattya Gyselle de Holanda e Silva, Julieta Genre, Anselmo Gomes de Oliveira, Eryvaldo Sócrates Tabosa do Egito, "Understanding Drug Release Data through Thermodynamic Analysis", Materials, 10, 651, Pages 1-17, 2017.

[28]. Fang, Huayang, "The kinetics of drug dissolution in polymers during hot-melt extrusion", Theses, New Jersey Institute of Technology, 229, (2015).

Figures

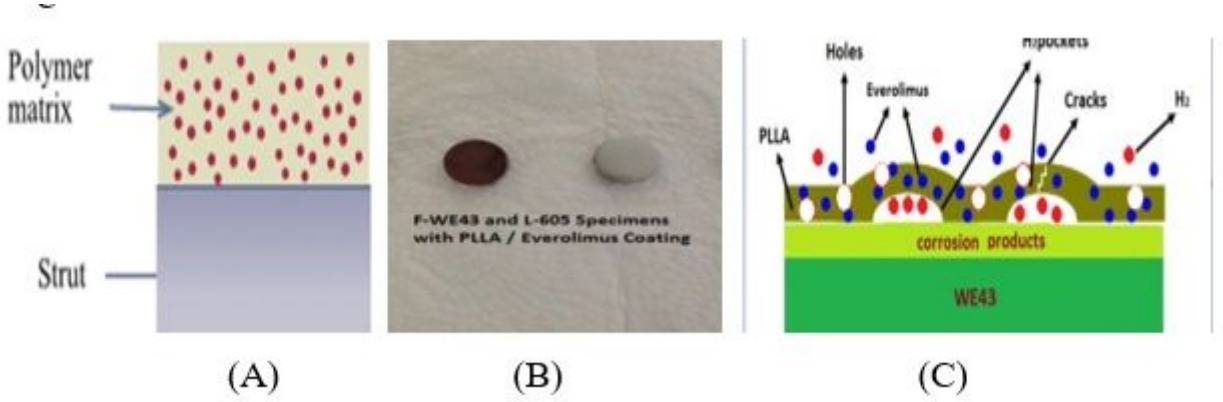

Figure 1

(A) Polymer-drug on a substrate, (B) PEF-WE43 and PE-L605 samples, and (C) the Mg degradation effect on the PLLA/EVRO layer.

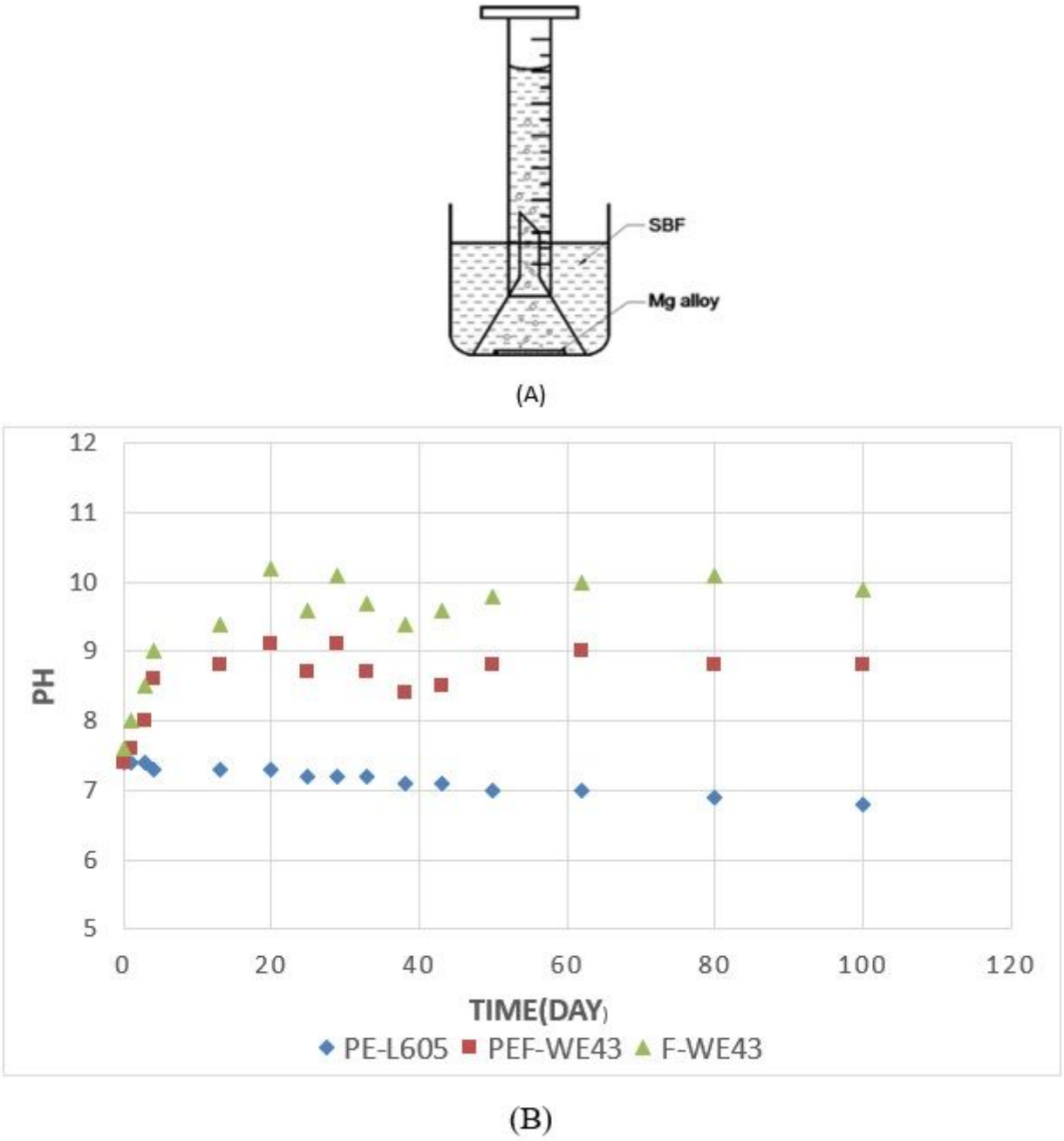

Figure 2

(A) Hydrogen evolution, and (B) pH media change of PE-L605, PEF-WE43 and F-WE43 due to the magnesium degradation during 100 days of immersion in the SBF.

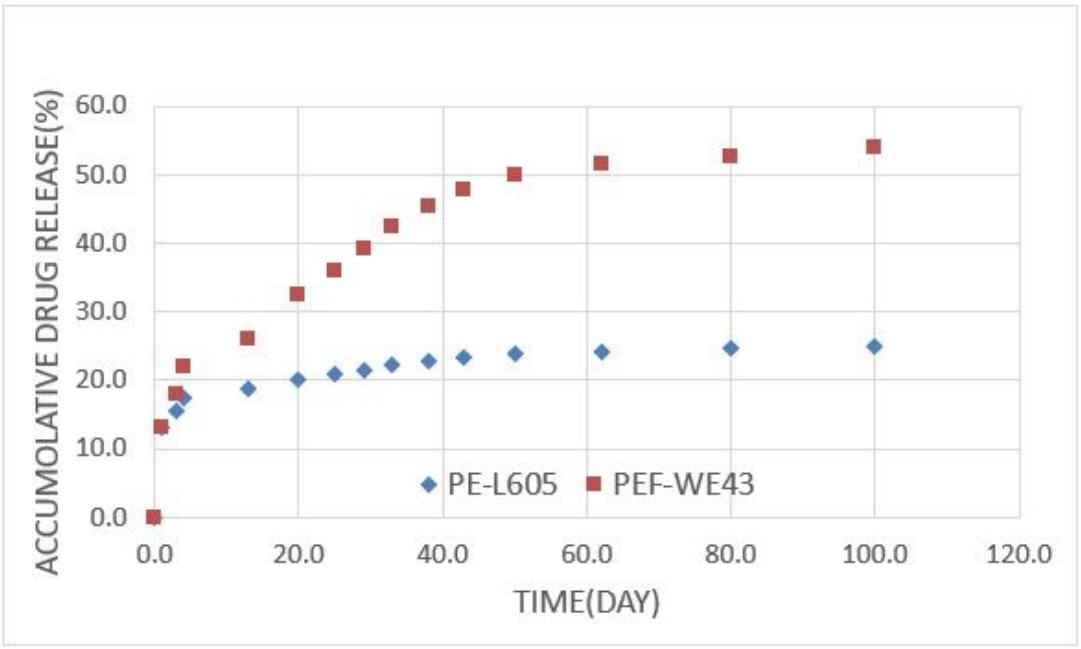

(A)

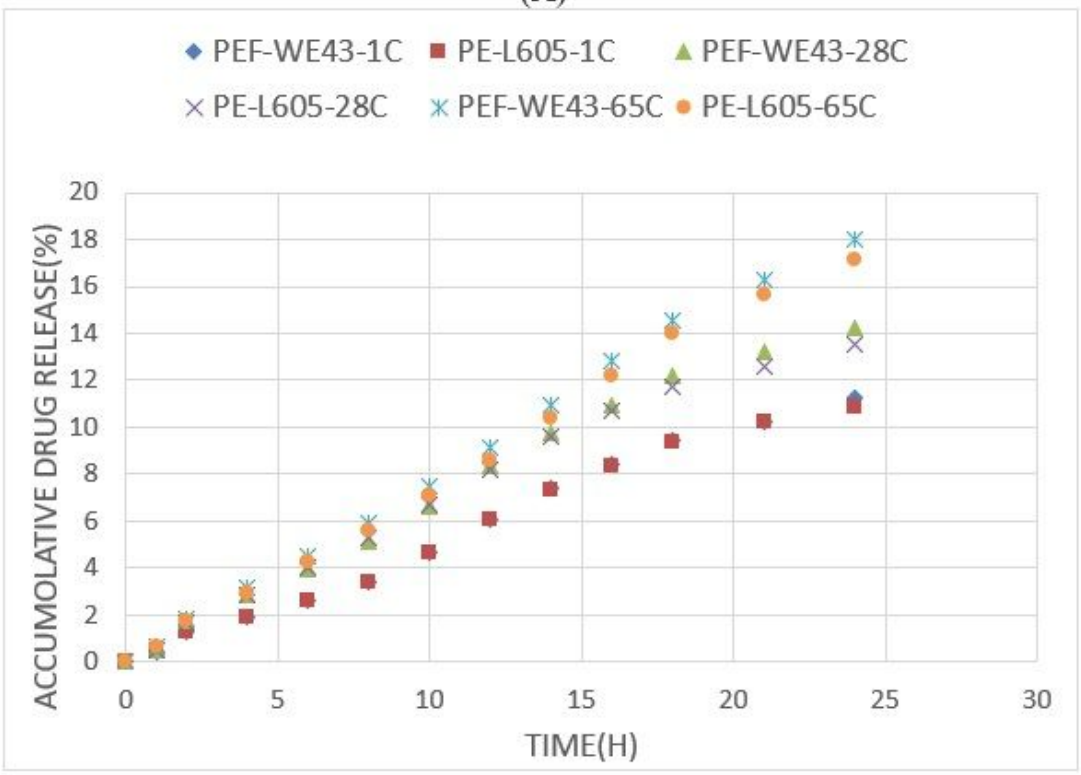

(B)

Figure 3

Cumulative Everolimus release from: (A) PE-L605 and PEF-WE43 during 100 days, and (B) PEF-WE43 and PE-L605 in the first 24 hours of immersion at 1ºC, 28ºC and 65ºC.

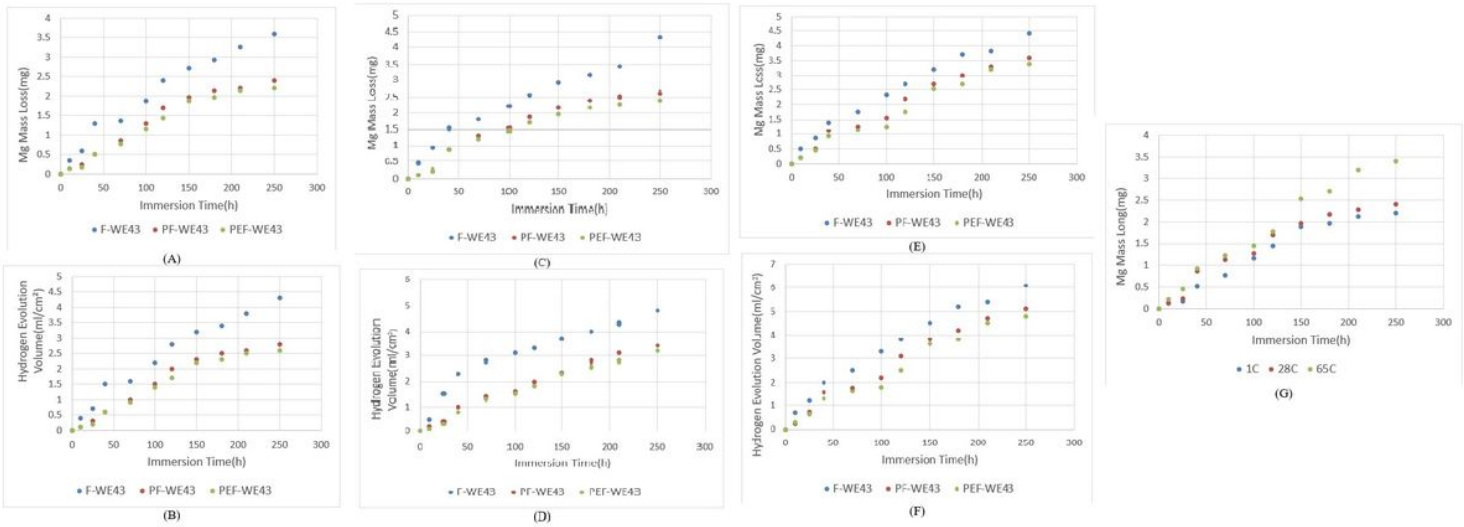

Figure 4

Mass loss (A, C, E) and hydrogen release (B, D, F) from different specimens at 1, 28, and 65ºC, respectively. (G) Mass loss diagram of PEF-WE43 specimen at 1, 28, 65ºC.

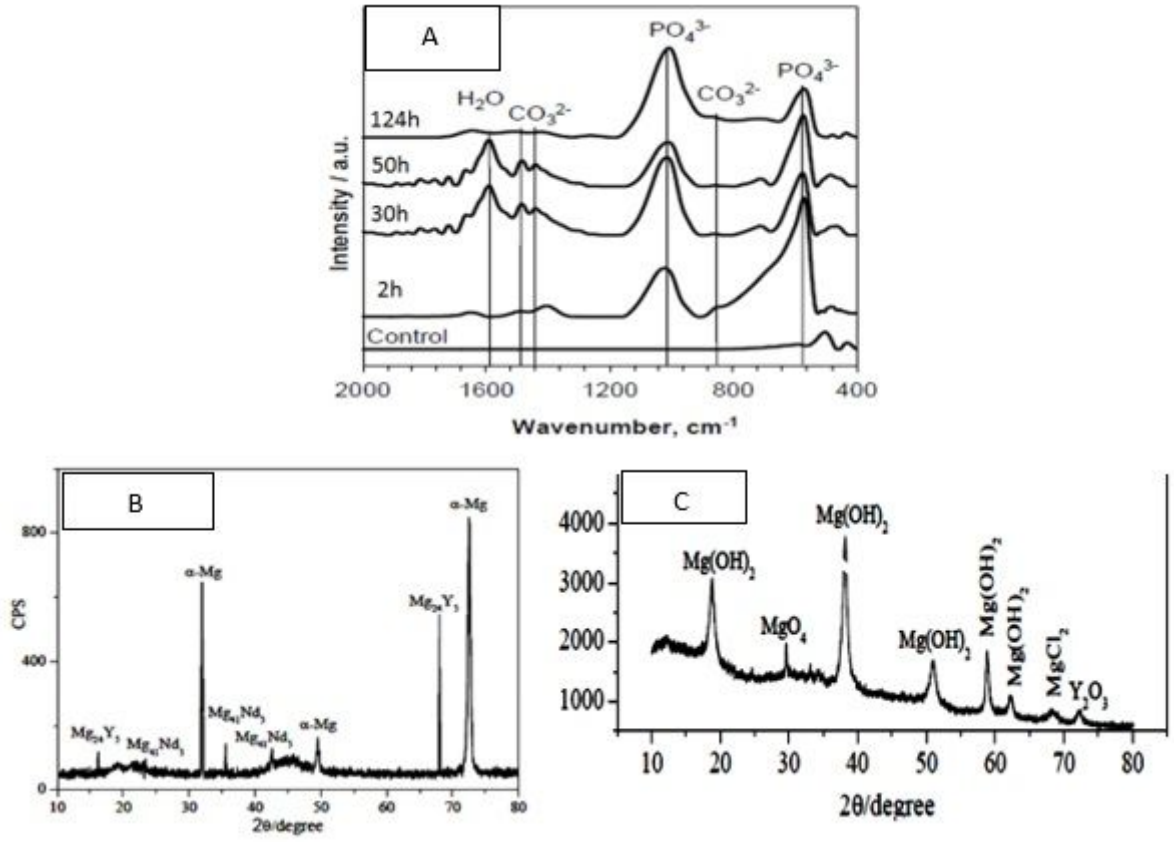

Figure 5

(A) ATR-FTIR spectrum of WE43 magnesium alloy immersed in SBF different times showing the presence of functional groups, carbonates, and phosphates. A polished WE43 specimen was used as the control

specimen. (B) X-ray diffraction pattern of WE43 alloy before immersion, and (C) XRD analysis of corrosion products of WE43 alloy immersed in SBF after 30 days.

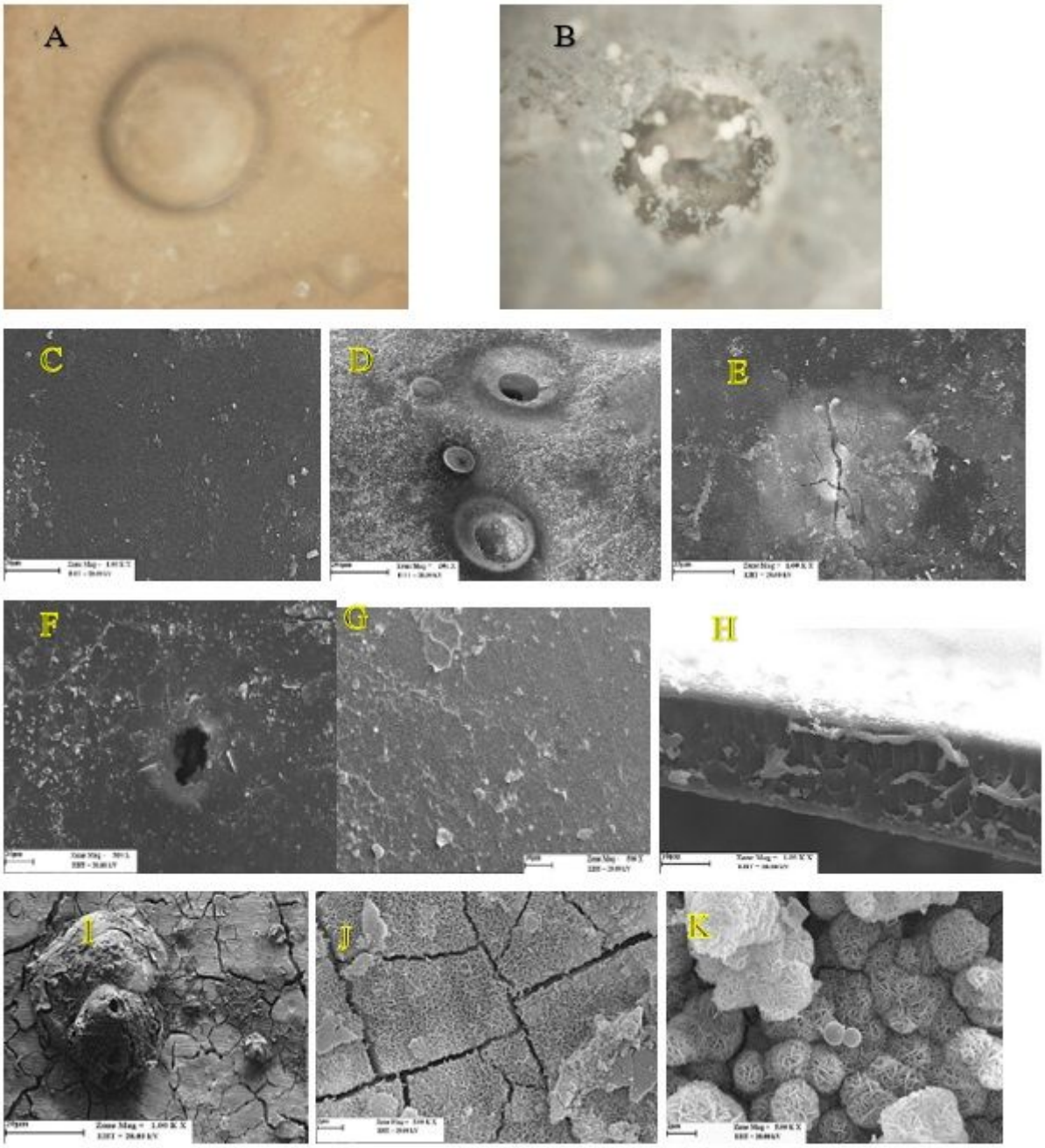

Figure 6

Blisters (A) formed by hydrogen bubbles inside the PLLA due to the magnesium-water reaction under the layer after six days (100x magnification), and (B) partial destruction of the coating after 14 days (100x magnification). And SEM micrograph of the WE43-PLLA specimen immersed in SBF for: (C) one day, (D) 20 days, (E) 30 days, and (F) 40 days. (G) L605 coating surface after 40 days immersion. (H) SEM micrograph of the cross section of the PLLA coating. (I) Corroded surface of WE43 magnesium alloy immersed in SBF for 30 h. (J and K) SEM image of the corrosion products on the PLLA coating of WE43

sample immersed for 20 days in SBF. The geometric shape and volume of the corrosion product show physical damage to the PLLA. It is, therefore, well suited to release the drug.

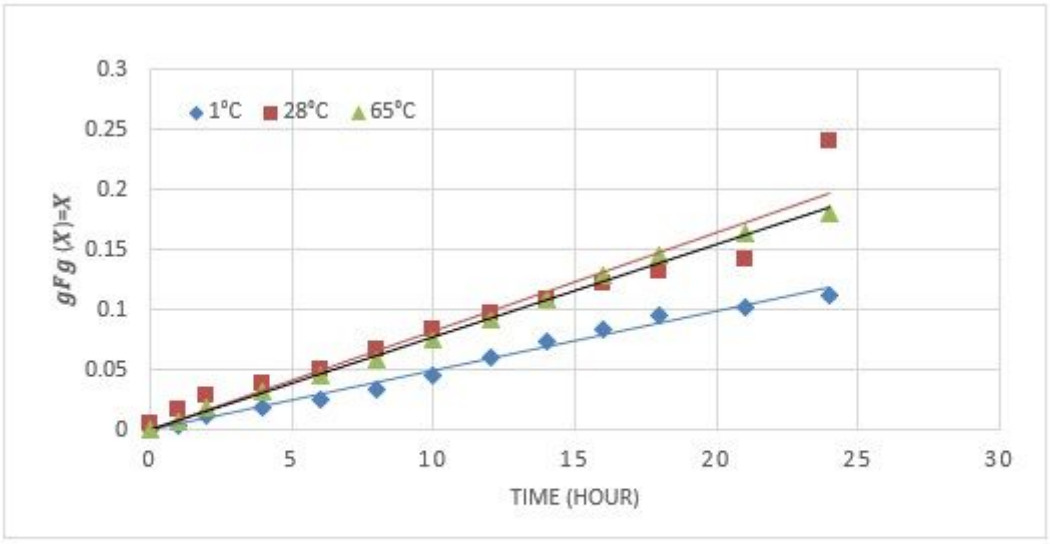

(a)

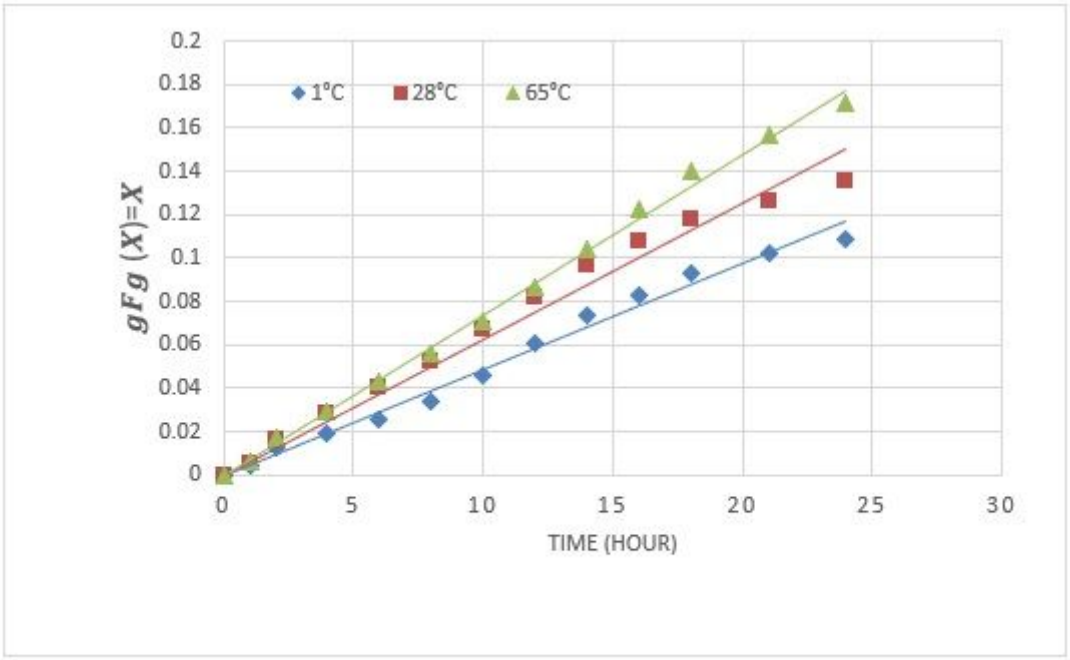

(b)

Figure 7

Comparison of the experimental release data (geometric shapes) with the model results (lines) for (a) PEF-WE43, and (b) PE-L605 samples during the first 24 hours of immersion.